



CHARACTERIZING THE ANISOTROPIC TENSILE BEHAVIOR AND DUCTILITY OF FFF-PRINTED ABS BASED ON PRINT DIRECTION AND RASTER ORIENTATION

ELDeeb I. S., Ehssan Esmael, and Abdelhameed A. Zayed

**Production Engineering and Mechanical Design Department, Faculty of Engineering,
Tanta University, Tanta, 31521, EGYPT.**

ABSTRACT

Fused Filament Fabrication (FFF) of Acrylonitrile Butadiene Styrene (ABS) produces components with significant mechanical anisotropy, critically impacting their reliability in load-bearing applications. This study comprehensively characterizes how both printing direction (Flat, On-Edge, Up-Right) and raster orientation angle (systematically varied from 0° to 90°) govern the uniaxial tensile strength and ductility (strain at failure) of FFF-ABS. ASTM D638 Type IV specimens were fabricated with consistent parameters (50% infill), varying only these orientations, followed by tensile testing and optical fractography.

Profound anisotropy was confirmed. Printing direction established distinct performance tiers: Flat yielded the highest potential strength, On-Edge was intermediate, while Up-Right consistently demonstrated the lowest strength and minimal ductility due to brittle inter-layer delamination. The raster orientation angle acted as a critical modulator, particularly for Flat and On-Edge. In the Flat direction, 0° raster alignment maximized strength, whereas 90° minimized it; notably, intermediate angles (e.g., $\pm 45^\circ$) suggested enhanced ductility, highlighting a tunable strength-ductility trade-off. On-Edge properties also showed significant raster angle sensitivity. Conversely, Up-Right behavior remained largely insensitive to raster angle, dominated by interface weakness. Fractographic analysis correlated failure mechanisms with mechanical outcomes: delamination in Up-Right samples, mixed inter/intra-raster failure in On-Edge, and distinct raster-angle-dependent modes (inter-raster vs. intra-raster) in Flat samples. This research underscores that optimizing FFF-ABS requires careful selection of both printing direction and raster angle to achieve the targeted balance between tensile strength and ductility for specific engineering requirements.

KEYWORDS

Acrylonitrile Butadiene Styrene (ABS), Fused Filament Fabrication (FFF), Additive Manufacturing (AM), Tensile Strength, Ductility, Anisotropy, Build Orientation, Raster Angle, Fractography.

INTRODUCTION

Additive Manufacturing (AM) technologies have transitioned from primarily rapid prototyping tools to viable methods for direct manufacturing of functional components across a multitude of industries. The biomedical, automotive, food, construction, aerospace, and other industries have shown the greatest interest in additive manufacturing in recent years, [1 - 5]. Design freedom is provided by AM, which implies that intricate geometries can be produced in a single step, obviating the need for expensive equipment and postprocessing procedures like machining, [6]. Additionally, AM allows for the one-step manufacturing of several components, which lowers the end product's weight. Because the final product may be produced close to the consumer, additive manufacturing (AM) offers supply chains several financial advantages, such as reduced material waste, streamlined production procedures, and more flexibility. Among the diverse AM processes, Fused Filament Fabrication (FFF), a material extrusion technique, has gained significant traction due to its inherent advantages: relatively low equipment cost, operational simplicity, material versatility, and the capability to produce parts with complex geometries directly from computer-aided design (CAD) data with minimal human intervention, [7, 8]. Within the portfolio of materials compatible with FFF, Acrylonitrile Butadiene Styrene (ABS) holds a prominent position. It is frequently chosen for engineering applications owing to its favorable combination of mechanical robustness, including good impact strength and toughness, adequate thermal resistance for many environments, and overall cost-effectiveness compared to higher-performance engineering thermoplastics [9, 10]. These attributes make ABS workhorse material for functional prototypes and numerous end-use applications produced via FFF.

By layering extruded materials, such as ABS plastic, Fused Filament Fabrication (FFF) creates parts with intricate geometries. The process involves depositing filaments of the material in a semi-molten state. In a temperature-controlled build environment, the partially melted filament is extruded through a heated nozzle and placed onto the partially produced item in the form of a predetermined two-dimensional (x-y) layer pattern as clear in Fig. 1. After being extruded and set in tracks while molten, the freshly deposited material fuses with the nearby previously installed material. Once a layer is completely deposited, the next layer is deposited on top of it as the build platform descends along the z-axis in increments equal to the filament height (layer thickness), [11].

The layered components' mechanical characteristics must be equal to those of parts made using conventional manufacturing methods and satisfy service loads and operational criteria. In contrast to traditional manufacturing methods, the attributes of additively manufactured parts can be influenced by process and structural factors as opposed to just material characteristics. This is also the primary drawback of using functional components made from FDM printed parts. Anisotropy may arise as a result of this process' impacts, such as the delamination of the component layers or materials. Furthermore, printed parts usually have lower elastic qualities than injection-molded parts made of the same thermoplastics. As a result, designers are

unable to depend on data from static material databases, making the process of choosing materials more difficult.

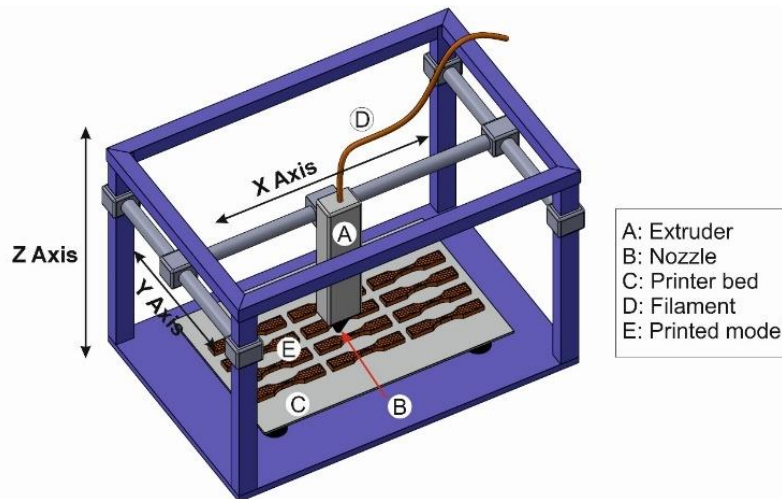


Fig. 1 Schematic of the 3D printing process.

FDM's high anisotropy and poor interlayer bonding, however, are major disadvantages that lead to printed parts failing as a result of delamination, buckling, bending, and shearing, [12]. Studying the printing parameters that may impact the mechanical qualities under various loading scenarios is therefore essential to maximizing the potential of FDM 3D printing technology. Previous investigations of printing process parameters considered printing temperature, [13], layer thickness, [14], contour layers, [15], printing orientation, [16], printing speed [17], raster gap [10], [14], raster width, [18], and raster orientation, [12, 14]. The influence of different combinations of air gap and raster angles on the mechanical properties of ABS was studied by Daoud et al., [10]. The results showed that the mechanical properties of the 3D printed ABS and the injection molded are similar. Ahne et al., [11] investigated the effect of model temperature, bead width, air gap, and raster orientation on the compressive and tensile strengths of FDM build ABS to be compared with the injection molded ABS P400.

Moreover, Dhinesh et al., [19] examined the tensile and flexural characteristics of ABS, PLA, and PLA-ABS specimens. The prediction of the FDM parts' tensile strength based on an analytical model was introduced by Ahne et al., [20]. In a comparative study, Wu et al., [21] examined how raster angle and layer thickness affect the ABS and polyether-ether-ketone (PEEK). The impact of raster-to-raster gap, layer thickness, and orientation on ABS and PLA parts fabricated by different commercial 3D printers was described by Tymrak et al., [22]. Rezaeian et al., [17] investigated how the fracture and tensile properties of FDM ABS specimens are affected by the printing speed. In addition, the directional dependency (anisotropy) related to build orientation (up-right versus flat/on-edge) is also well-acknowledged and has been documented for ABS and other materials, [9, 11, 23 - 30].

However, a gap exists in the literature regarding a systematic and comprehensive

investigation that simultaneously evaluates the effect of the three primary build directions, namely; up-right (load perpendicular to layers), on-edge (layers vertical, load parallel to layers), and flat (layers parallel to the major plane) and a detailed range of in-plane raster orientation angles (beyond the commonly studied 0° , 45° , 90°) on the static uniaxial tensile properties of ABS. While individual aspects have been studied, a direct comparison across this full matrix of orientations, using consistent material and baseline processing parameters, is less prevalent. Such data is essential for creating a more complete map of ABS anisotropic behavior under tensile load. Additionally, directly correlating these quantitative mechanical results with qualitative fractographic analysis for each specific orientation combination provides crucial insights into the underlying failure mechanisms (e.g., delamination dominance vs. inter-raster failure vs. filament fracture) that govern the observed properties. This study aims to address this gap by providing such a detailed experimental dataset and analysis, while focusing on the static uniaxial tensile properties of a specific commercial ABS filament processed using a defined FFF printer and a consistent set of baseline printing parameters (including 50% infill density, 0.25 mm layer height, 45 mm/s speed). The primary variables are the build direction and the raster orientation angle.

The subsequent sections of this paper are outlined as follows. Detailed materials and methods are presented in Section 2, while the comprehensive experimental results focusing on tensile strength, ductility, and fractography are introduced in Section 3. An in-depth discussion interpreting the findings of this work are found in Section 4. Finally, the main conclusions summarizing the key contributions and implications are shown in Section 5.

MATERIALS AND METHODS

This section details the materials, specimen design, fabrication process, experimental setup, and analysis techniques employed to investigate the influence of printing direction and building orientation angle on the tensile properties of FFF-processed ABS.

Material and Geometry of Test Specimen

ABS supplied as a 1.75 mm diameter filament by Bestfilament (Moscow, Russia). ABS is an amorphous engineering thermoplastic widely employed in FFF due to its advantageous mechanical profile, which includes notable toughness, impact resistance, and dimensional stability under moderate thermal conditions, [10, 31]. To ensure the reliability and comparability of the tensile testing results, all specimens were designed and fabricated in accordance with the specifications outlined in the ASTM D638 standard, "Standard Test Method for Tensile Properties of Plastics", [32, 33]. Specifically, the Type IV specimen geometry, commonly referred to as a "dog-bone" shape, was adopted, [34, 35] as shown in Fig. 2. This geometry is particularly suitable for characterizing the tensile response of materials produced via layer-by-layer processes like FFF, as it provides a defined gauge section where deformation and failure are expected to concentrate, [35]. The digital model for the specimen was created using Solidworks™ computer-aided design (CAD) software

and subsequently exported as a stereolithography (.STL) file, the standard format for interfacing with FFF slicing software. While adhering to the critical gauge length and overall form of the Type IV standard, all specimens were printed with a consistent nominal thickness of 4.0 mm.

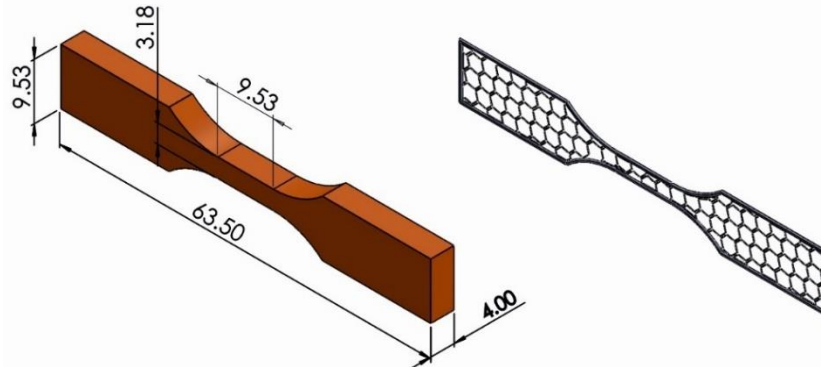


Fig. 2 Standard tension specimen dimensions with honeycomb structure.

A KINGROOM KLP1 3D Printer served as the FFF platform for producing all tensile specimens. This system is equipped with key features necessary for processing ABS reliably: a single extrusion head compatible with 1.75 mm filament, a temperature-controlled heated build platform, and an enclosed build chamber. The heated platform is critical for promoting adhesion of the initial ABS layers and minimizing temperature gradients that cause warping, [36]. The enclosed chamber maintains a moderately elevated and stable ambient temperature (controlled around 60°C for this study, Table 1) during the printing process, which further mitigates differential shrinkage, reduces residual stresses, and potentially enhances inter-layer bond quality by slowing cooling rates, [36].

Slicing and Toolpath Parameterization

Generation of the machine-specific instructions (G-code) from the .STL model was performed using the open-source Polygon slicing software. This crucial step involves digitally "slicing" the model into discrete layers and defining the precise toolpath the extrusion nozzle will follow for each layer, including perimeter contours and internal infill patterns. A core aspect of this study involved using the slicer to rigorously control the build direction and the raster orientation angle, while keeping other parameters constant. The baseline printing parameters, selected based on established practices for ABS FFF [36], [37], preliminary optimization, and settings used in related reference, were maintained consistently for all prints as listed in table 1 to isolate the variables of interest.

Table 1 Fixed printing conditions and parameters

Parameter	Value
Nozzle diameter	0.25 mm
Layer height	0.25 mm
Extrusion temperature	230 °C
Build Platform temperature	110 °C

Build chamber temperature	60 °C (controlled ambient)
Printing speed (Infill/Perimeter)	45 mm/s
Infill shape	Honeycomb
Infill density	50%
Number of perimeter shells	2
Shell thickness	0.5 mm
Infill raster orientation	Default $\pm 45^\circ$ (relative to the specified building orientation angle)

Build Directions and Orientation Angles

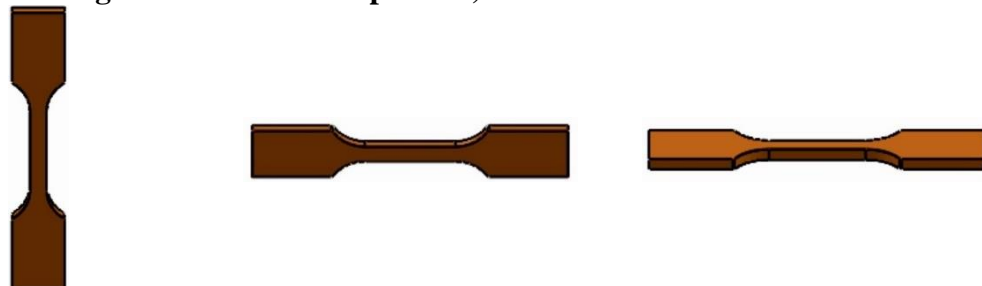
This study employed a systematic experimental design to evaluate the anisotropic tensile response of FFF-ABS. Two primary factors were varied:

Printing Direction (Build Direction): This refers to the overall orientation of the specimen relative to the build platform during fabrication. Three distinct directions shown in Fig. 2 were investigated as follows:

- **Flat (F):** The specimen's largest face (defined by length and width) was parallel to the build platform (XY plane). Layers accumulated along the Z-axis (thickness direction).
- **On-Edge (OE):** The specimen stood on one of its long, narrow side edges. Layers were deposited vertically relative to the platform, accumulating along the X or Y axis.
- **Up-Right (UR):** The specimen stood vertically on one of its small ends. Layers were parallel to the build platform (XY plane), accumulating along the Z-axis (major length direction).

Building Orientation Angle (Raster Angle): For each printing direction, the orientation of the specimen's longitudinal axis relative to the printer's primary movement axis (e.g., X-axis) was varied. This implicitly controls the angle between the applied tensile load and the primary direction of the infill rasters within each layer. The angle pairings investigated were $[0^\circ, 90^\circ]$, $[15^\circ, 75^\circ]$, $[30^\circ, 60^\circ]$, and $[45^\circ, -45^\circ]$. These pairings effectively cover the spectrum of relative angles from parallel (0°) to perpendicular (90°) between the tensile axis and the primary coordinate system influencing raster deposition.

To ensure robust statistical analysis, three replicate specimens were fabricated and tested for every unique combination of printing direction and building orientation angle, resulting in a comprehensive dataset derived from 63 individual tensile tests (3 directions \times 7 angle conditions \times 3 replicates).



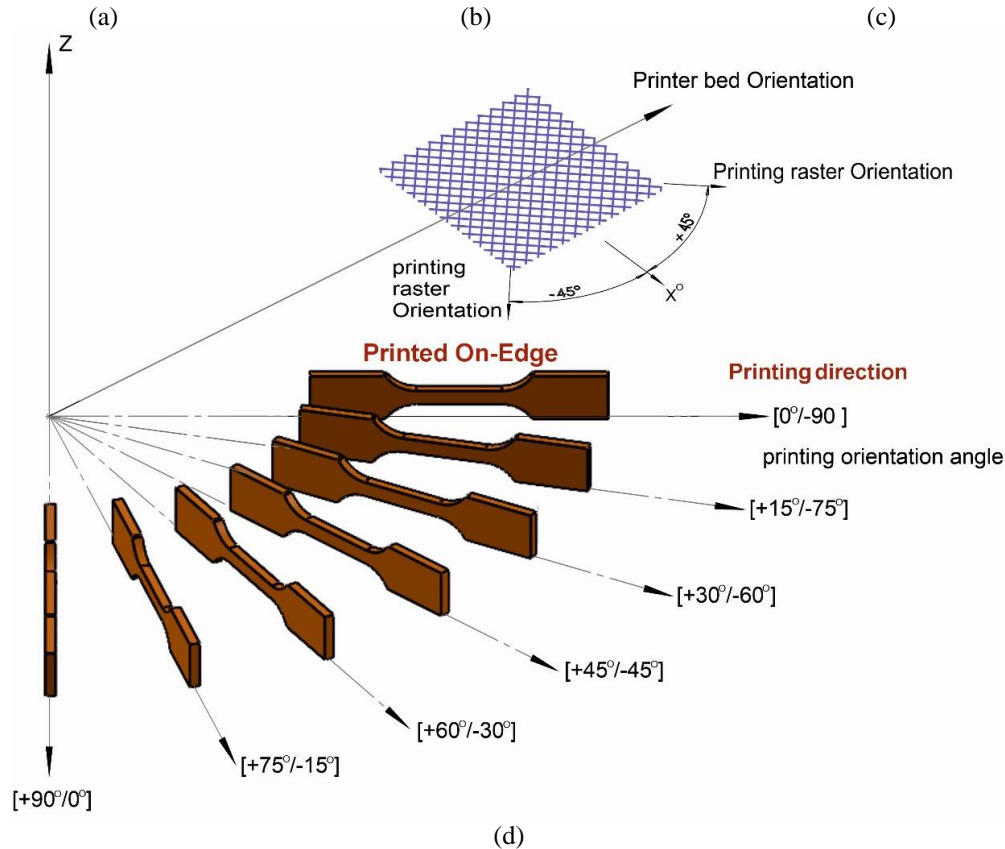


Fig. 3 Test specimen (a) Up-right, (b) On-edge, (c) Flat, and (d) On-edge with different orientation angles.

Uniaxial Tensile Testing Procedure

Uniaxial tensile tests were conducted using a universal testing machine (UTM), likely a SHIMADZU system equipped with a 100 kN load cell, following the guidelines of ASTM D638 [32], [33]. Each specimen was carefully aligned and secured in the wedge-action grips of the UTM to ensure load application along the longitudinal axis and minimize bending moments. Tests were performed at a constant crosshead displacement rate of 5 mm/min under ambient laboratory conditions (approximately 23°C). Load (Force) and crosshead displacement data were recorded continuously throughout each test at a sampling rate of 100 Hz using the testing machine's integrated data acquisition system and control software. The recorded load-displacement data was processed to calculate key tensile properties for each specimen. Engineering stress was calculated by dividing the load by the initial cross-sectional area of the gauge section. Engineering strain was calculated from the crosshead displacement relative to the initial gauge length. The primary metrics determined were:

- **Ultimate Tensile Strength (UTS):** The maximum engineering stress sustained by the specimen during the test.
- **Strain at Failure (Elongation at Break):** The engineering strain corresponding to the point of specimen fracture.
- Mean values and standard deviations for UTS and strain at failure were

calculated for the three replicates within each condition group.

Figure 4 shows the actual printed ABS specimen before and after performing the tension test.

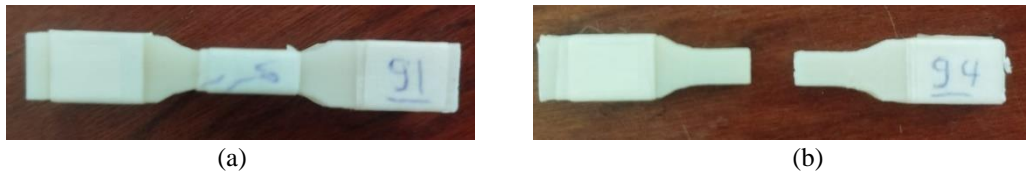


Fig. 4 Printed ABS specimen (a) before the tensile test (b) after the tensile test.

RESULTS

Effect of different building orientation angles on tensile strength in Up-Right direction. Figure 5 presents the complete set of stress-strain curves obtained from tensile tests on ABS samples printed in the Up-Right direction, encompassing all tested building orientation angles (likely 0° through 90° , based on typical studies). Figure 6 selectively displays representative curves from this set to illustrate the general trends more clearly. These curves visually demonstrate the mechanical response of the material under tensile load when force is applied perpendicular to the printed layers. Typically, this orientation yields the lowest tensile strength due to stress being concentrated on the weaker inter-layer bonds. Variations between the curves within Fig. 5 highlight the inherent variability in the FFF process, even for nominally identical parameters, and also show the influence of changing the in-plane raster orientation angle relative to the sample's geometry, although the primary failure mechanism remains inter-layer separation.

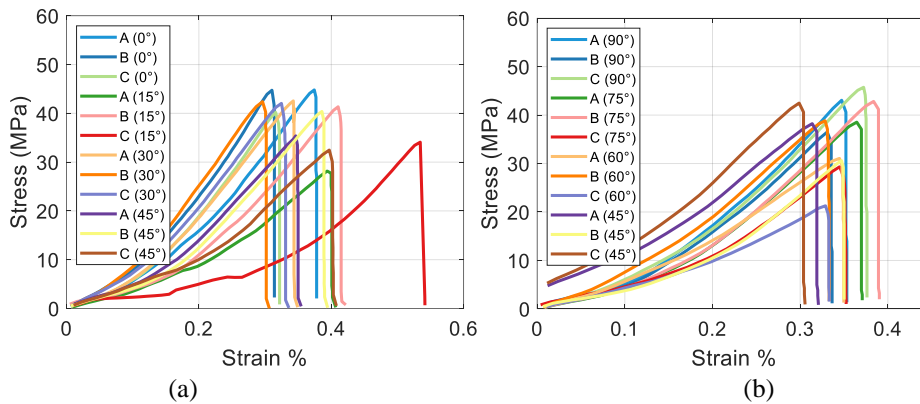


Fig. 5 Stress-Strain curves for all ABS samples printed in the Up-Right direction with varying building orientation angles (0° to 90°). (a) Samples with printing angle from 0° to 45° , and (b) Samples with printing angle from 45° to 90° .

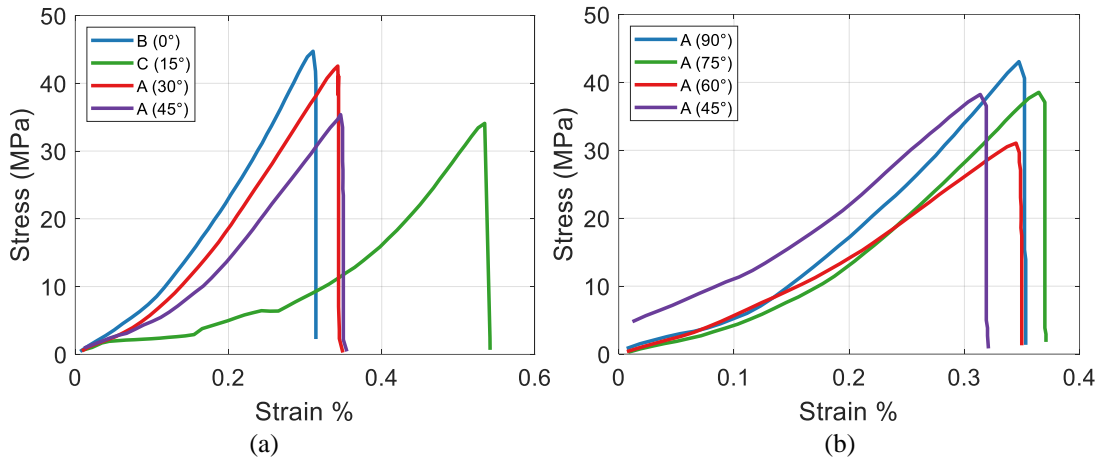


Fig. 6 Selected representative Stress-Strain curves for ABS samples printed in the Up-Right direction, illustrating trends across different building orientation angles. (a) Samples with printing angle from 0° to 45°, and (b) Samples with printing angle from 45° to 90°.

Table 2 quantitatively summarizes the tensile test results for the Up-Right printing direction, detailing the maximum, selected, minimum, and mean values for stress and strain at failure for each tested building orientation angle (0°, 15°, 30°, 45°, 60°, 75°, 90°). Figure 7 plots the tensile strength (maximum, selected, minimum, mean) against the orientation angle, while Fig. 8 shows the corresponding plot for strain at failure.

Table 2 Tensile properties (maximum, selected, minimum, and mean stress and strain) of ABS samples printed in the Up-Right direction for different building orientation angles.

Printing angle in Up-Right direction	Maximum stress ABS	Selected stress ABS	Minimum stress ABS	Mean stress ABS	Maximum strain ABS	Selected Strain ABS	Minimum Strain ABS	Mean Strain ABS
0° Model (1)	44.7998688	44.73598	40.22252	43.25279	0.377857	0.321892	0.314059	0.337936
15° Model (1)	41.3440285	34.09099	28.16058	34.53187	0.54143	0.421961	0.406774	0.456722
30° Model (1)	42.5511807	42.394	42.0403	42.32849	0.349283	0.335995	0.306435	0.330571
45° Model (1)	40.3842590	35.37997	32.46718	36.07714	0.407689	0.394553	0.354527	0.38559
45° Model (2)	42.4802938	38.23226	30.61813	37.11023	0.350103	0.320849	0.305571	0.325507
60° Model (2)	38.8304469	31.06436	21.28182	30.39221	0.349778	0.333208	0.333122	0.338703
75° Model (2)	42.8239340	38.54154	29.33452	36.9	0.390312	0.370796	0.352473	0.371194
90° Model (2)	45.7394478	43.06218	36.49337	41.765	0.376196	0.353224	0.336404	0.355275

Tensile Strength (Fig. 7), the data likely shows some fluctuation in tensile strength as the orientation angle changes, but overall strength remains relatively low compared to other printing directions. There might not be a strong, consistent trend with angle in this build direction because the primary failure mode (delamination) is governed by inter-layer adhesion, which is less directly affected by the in-plane raster angle compared to strength in Flat or On-edge directions. Any observed variations might relate to how internal stresses distribute or how edge contours interact with the raster pattern. Table 2 shows specific mean stress values ranging likely between ~30 MPa

and ~43 MPa, confirming the lower strength compared to typical bulk ABS or optimally printed FFF parts.

Strain at Failure (Fig. 8), similar to strength, the strain at failure (ductility) in the Up-Right direction is generally limited by the brittle nature of inter-layer failure. Figure 8 likely shows relatively low strain values with potential fluctuations depending on the angle. Angles that might induce slightly more complex stress states before delamination could show marginally higher strain, but overall elongation is expected to be poor. The mean strain values in Table 2 likely fall within a limited range, reflecting this characteristic.

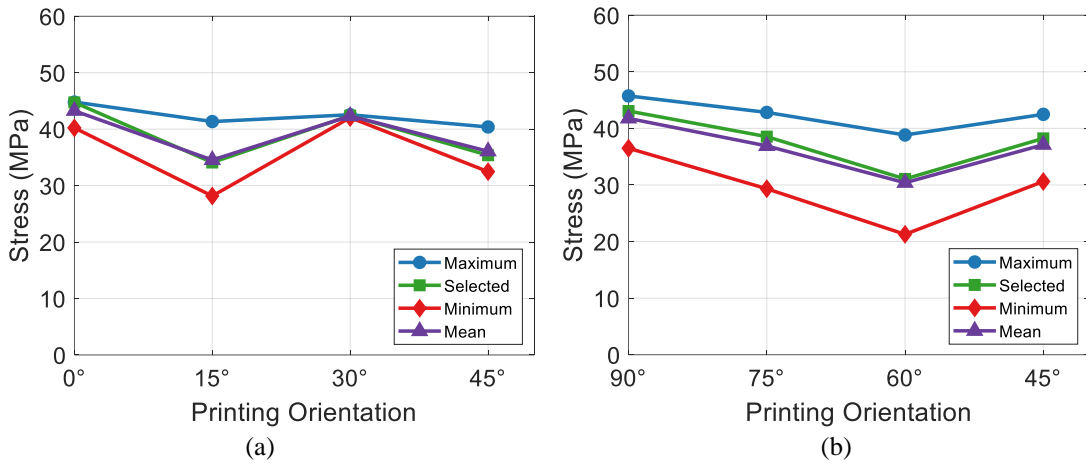


Fig. 7 Effect of building orientation angle on the tensile strength (maximum, selected, minimum, and mean) of ABS samples printed in the Up-Right direction. (a) Model (1) samples with printing angle from 0° to 45°, and (b) Model (2) samples with printing angle from 45° to 90°.

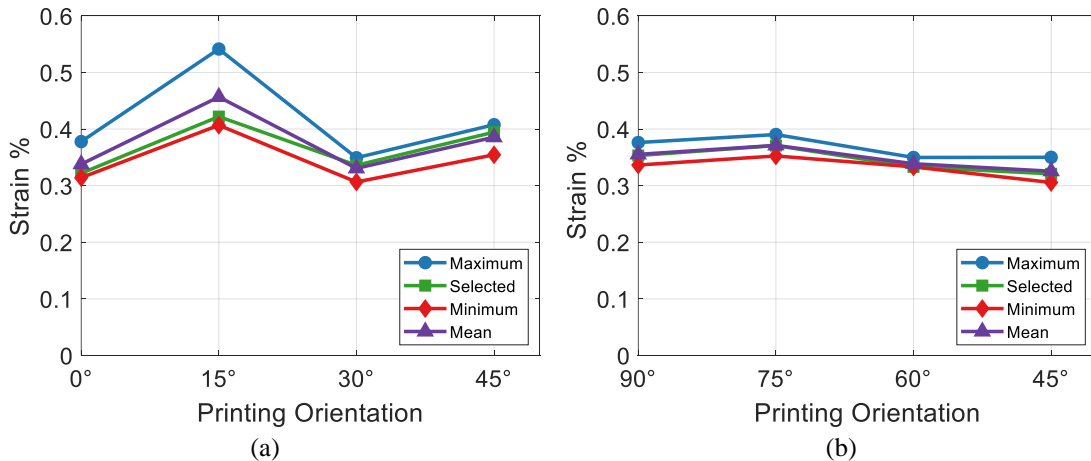


Fig. 8 Effect of building orientation angle on the strain at failure (maximum, selected, minimum, and mean) of ABS samples printed in the Up-Right direction. (a) Model (1) samples with printing angle from 0° to 45°, and (b) Model (2) samples with printing angle from 45° to 90°.

Effect of different building orientation angles on tensile strength in On-Edge direction.

Figure 9 displays all stress-strain curves for ABS samples printed in the On-Edge direction across the various orientation angles, while Fig. 10 shows selected representative curves. In this orientation, the tensile load is applied parallel to the layers but perpendicular to the build plate surface. The layers themselves are aligned vertically. This configuration typically yields intermediate mechanical properties. The strength relies on both the intra-layer strength of the filaments and the bonding between adjacent rasters within each layer, as well as the integrity of the vertically oriented layers.

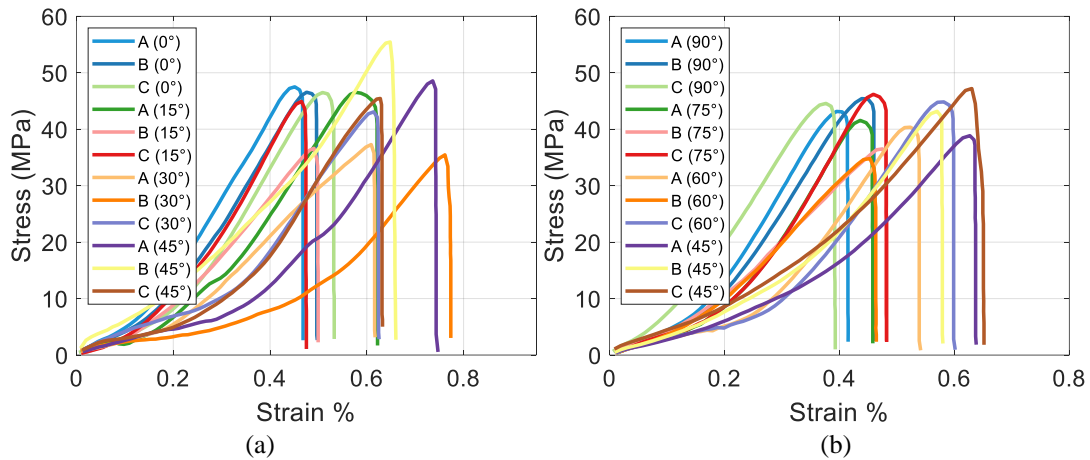


Fig. 9 Stress-Strain curves for all ABS samples printed in the On-Edge direction with varying building orientation angles (0° to 90°). (a) Samples with printing angle from 0° to 45° , and (b) Samples with printing angle from 45° to 90° .

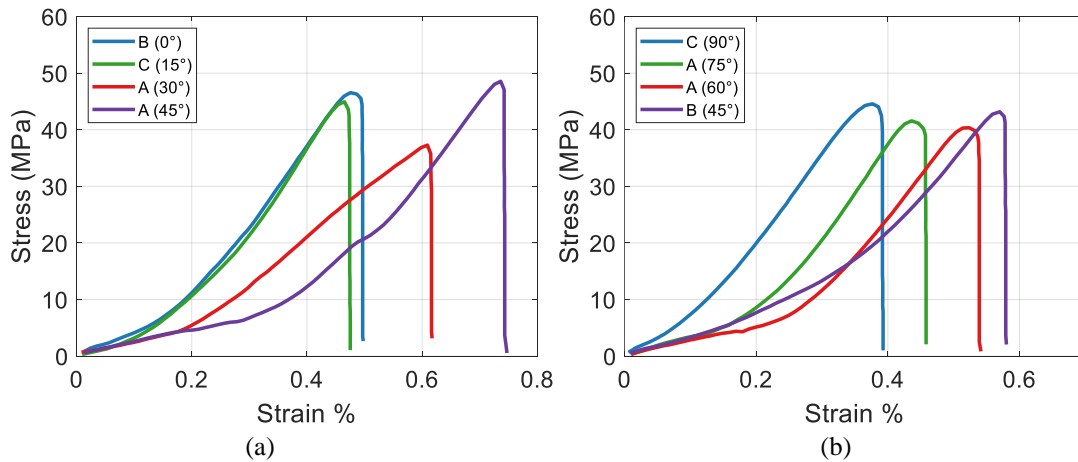


Fig. 10: Selected representative Stress-Strain curves for ABS samples printed in the On-Edge direction, illustrating trends across different building orientation angles. (a) Samples with printing angle from 0° to 45° , and (b) Samples with printing angle from 45° to 90° .

Table 3 provides the detailed tensile properties (max, selected, min, mean stress and strain) for the On-Edge direction as a function of the building orientation angle.

Figure 11 plots tensile strength versus angle, and Fig. 12 plots strain at failure versus angle.

Tensile Strength (Fig. 11), the strength in the On-Edge direction is expected to be significantly higher than Up-Right but potentially lower than the optimal Flat orientation. The trend with orientation angle is likely more pronounced here than in the Up-Right case. Angles where the rasters are more aligned with the load direction (e.g., 0° or small angles relative to the load axis within the vertical layers) might show higher strength, while angles where the load is applied across the bonds between adjacent vertical rasters (e.g., 90°) could be weaker. Table 3 shows mean stress values potentially ranging from ~38 MPa to ~50 MPa, illustrating this intermediate strength. There might be an optimal angle (perhaps 45° as suggested by the high max stress in the table) where stress distribution is favorable.

Strain at Failure (Fig. 12), ductility in the On-Edge orientation can be complex. Failure might involve filament breaking, inter-raster shearing, or layer splitting. Figure 12 likely shows fluctuating strain values. Angles providing better inter-raster bonding or allowing for more uniform stress distribution might exhibit higher strain. Table 3 indicates a relatively wider range of mean strain values (perhaps ~0.42 to ~0.68), suggesting sensitivity to the raster orientation within the vertical layers.

Effect of different building orientation angles on tensile strength in Flat direction. Figure 13 shows the complete set of stress-strain curves for samples printed in the Flat (XY) direction, where the largest surface of the specimen lies on the build plate and layers are parallel to this surface. Figure 14 presents selected curves. This orientation, particularly with rasters aligned with the load, is expected to yield the highest tensile strength as the load is carried primarily along the continuous extruded filaments.

Table 3 Tensile properties (maximum, selected, minimum, and mean stress and strain) of ABS samples printed in the On-Edge direction for different building orientation angles.

Printing angle in On-Edge direction	Maximum stress ABS	Selected stress ABS	Minimum stress ABS	Mean stress ABS	Maximum strain ABS	Selected Strain ABS	Minimum Strain ABS	Mean Strain ABS
0° Model (3)	47.5070811	46.55079	46.49843	46.8521	0.532652	0.497628	0.468227	0.499502
15° Model (3)	46.5387176	44.93204	36.61281	42.69452	0.622177	0.499409	0.475124	0.532237
30° Model (3)	43.0745668	37.28433	35.45801	38.60564	0.773567	0.625318	0.617136	0.672007
45° Model (3)	55.4493974	48.55763	45.44803	49.81835	0.747192	0.660082	0.632397	0.67989
45° Model (4)	47.2060326	43.17063	38.85357	43.07674	0.651568	0.638088	0.58008	0.623245
60° Model (4)	44.8385855	40.35473	34.79475	39.99602	0.601499	0.541349	0.464201	0.535683
75° Model (4)	46.1828793	41.56459	36.51302	41.42016	0.482175	0.48157	0.458067	0.473937
90° Model (4)	45.4202155	44.57078	43.1492	44.38007	0.461394	0.415255	0.39276	0.423136

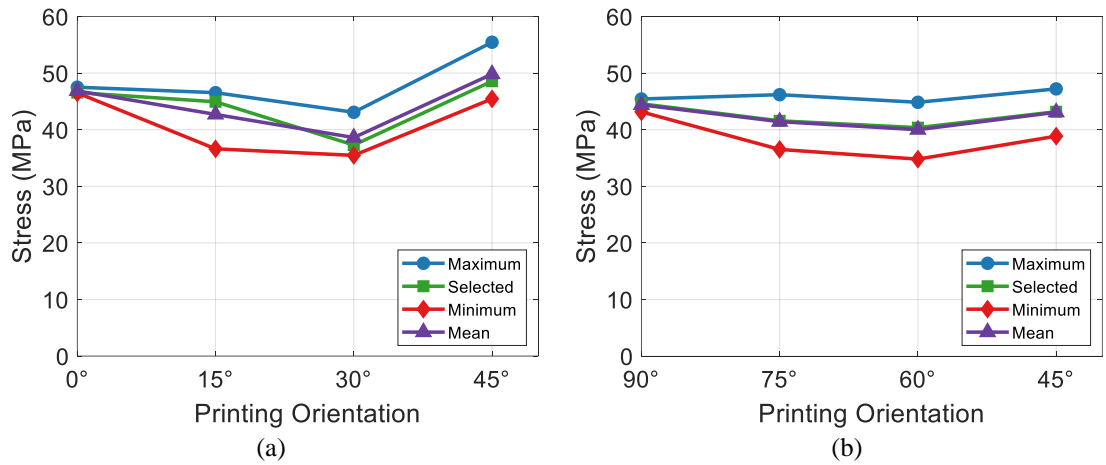


Fig. 11 Effect of building orientation angle on the tensile strength (maximum, selected, minimum, and mean) of ABS samples printed in the On-Edge direction. (a) Model (3) samples with printing angle from 0° to 45°, and (b) Model (4) samples with printing angle from 45° to 90°.

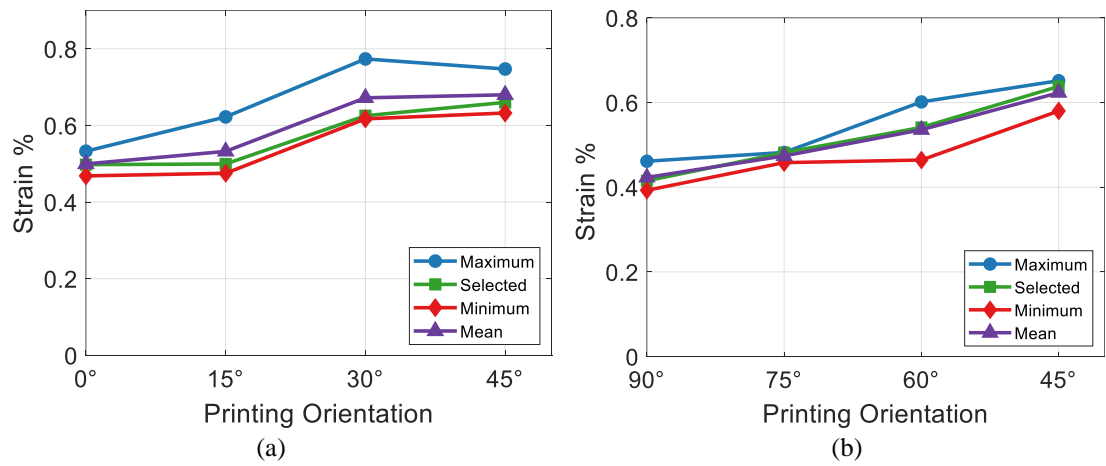


Fig. 12 Effect of building orientation angle on the strain at failure (maximum, selected, minimum, and mean) of ABS samples printed in the On-Edge direction. (a) Model (3) samples with printing angle from 0° to 45°, and (b) Model (4) samples with printing angle from 45° to 90°.

Table 4 details the tensile properties for the Flat direction across different orientation angles (0° to 90° relative to the tensile axis). Figure 15 plots tensile strength versus orientation angle, and Fig. 16 plots strain at failure.

Tensile Strength (Fig. 15), this orientation is expected to show the strongest dependence on the raster orientation angle. Strength should be highest when rasters are aligned with the tensile axis (0°), lowest when perpendicular (90°), and intermediate at other angles (like 45°). In the 0° case, failure requires breaking the filaments (intra-raster). In the 90° case, failure relies on the bonds *between* adjacent parallel filaments within a layer (inter-raster). The ±45° orientation often provides a good balance. Table 4 likely reflects this, with mean stress potentially highest near 0°

or 15°/75° (depending on exact alignment) and lowest near 90°. The overall strength values should be the highest among the three build directions, potentially reaching closer to bulk ABS properties in the optimal orientation.

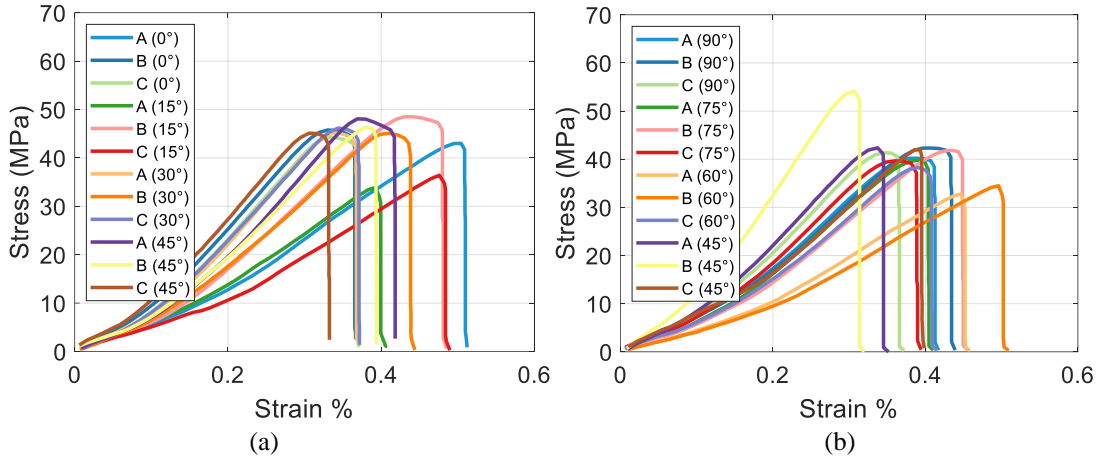


Fig. 13 Stress-Strain curves for all ABS samples printed in the Flat direction with varying building orientation angles (0° to 90°). (a) Samples with printing angle from 0° to 45°, and (b) Samples with printing angle from 45° to 90°.

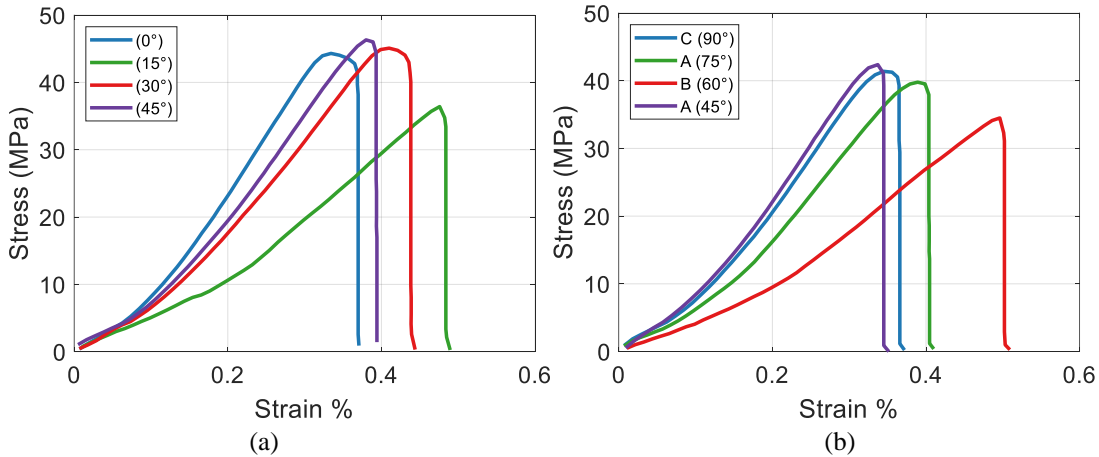


Fig. 14 Selected representative Stress-Strain curves for ABS samples printed in the Flat direction, illustrating trends across different building orientation angles. (a) Samples with printing angle from 0° to 45°, and (b) Samples with printing angle from 45° to 90°.

Strain at Failure (Fig. 16), ductility in the Flat direction should also depend strongly on the angle. The 0° orientation might exhibit moderate ductility associated with filament stretching. The ±45° orientation often shows good ductility due to shear yielding between filaments. The 90° orientation might be more brittle, failing at the weaker inter-raster interfaces. Figure 16 and Table 4 likely show this variation, with potentially higher strain values at 0° or ±45° compared to 90°.

Table 4 Tensile properties (maximum, selected, minimum, and mean stress and strain) of ABS samples printed in the Flat direction for different building orientation angles.

Printing angle in Flat direction	Maximum stress ABS	Selected stress ABS	Minimum stress ABS	Mean stress ABS	Maximum strain ABS	Selected Strain ABS	Minimum Strain ABS	Mean Strain ABS
0° Model (5)	45.77431883	44.30652	43.00171	44.36085	0.51209	0.370746	0.366565	0.416467
15° Model (5)	48.51707454	36.4094	33.87641	39.60096	0.489559	0.48554	0.405909	0.460336
30° Model (5)	45.13211013	45.08475	46.18042	45.46576	0.443928	0.371536	0.367764	0.394409
45° Model (5)	48.06869937	46.31582	45.1225	46.50234	0.418196	0.394175	0.33239	0.381587
45° Model (6)	54.14215467	42.37212	41.98418	46.16615	0.398413	0.351675	0.319705	0.356598
60° Model (6)	38.27249647	34.49696	32.77211	35.18052	0.509156	0.45824	0.414906	0.460767
75° Model (6)	41.87234016	39.77872	39.64372	40.4316	0.455675	0.410107	0.394316	0.420032
90° Model (6)	42.3230166	41.38198	40.20687	41.30395	0.438977	0.417028	0.371996	0.409334

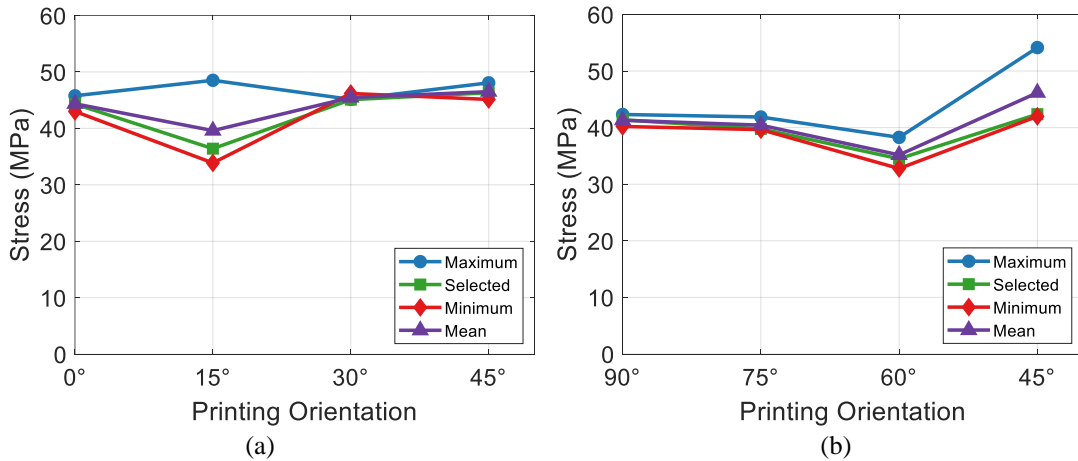


Fig. 15 Effect of building orientation angle on the tensile strength (maximum, selected, minimum, and mean) of ABS samples printed in the Flat direction. (a) Model (5) samples with printing angle from 0° to 45°, and (b) Model (6) samples with printing angle from 45° to 90°.

Comparison of the previous results depending on printing direction.

Table 5 consolidates the key mechanical property data (mean stress and mean strain) from Tables 2, 3, and 4, presenting a comprehensive overview of how both printing direction (Up-Right, On-Edge, Flat) and building orientation angle influence the tensile behavior of the FFF-printed ABS samples. It serves as a central reference for comparing the performance across all tested configurations.

Figure 17 compares the mean tensile strength across all tested orientation angles for the three different printing directions (Up-Right, On-Edge, Flat). Figure 18 provides the same comparison for mean strain at failure. These plots synthesize the overall findings.

Strength Comparison (Fig. 17), this plot clearly illustrates the anisotropy resulting from the build direction. It will show that the Flat direction consistently yields the

highest mean tensile strength, followed by On-Edge, with Up-Right being significantly weaker across all or most orientation angles.

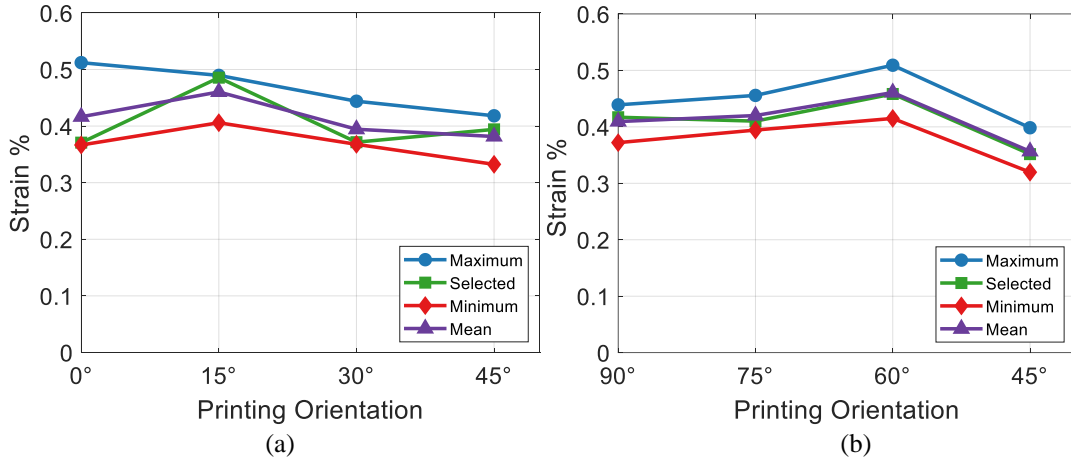


Fig. 16 Effect of building orientation angle on the strain at failure (maximum, selected, minimum, and mean) of ABS samples printed in the Flat direction. (a) Model (5) samples with printing angle from 0° to 45°, and (b) Model (6) samples with printing angle from 45° to 90°.

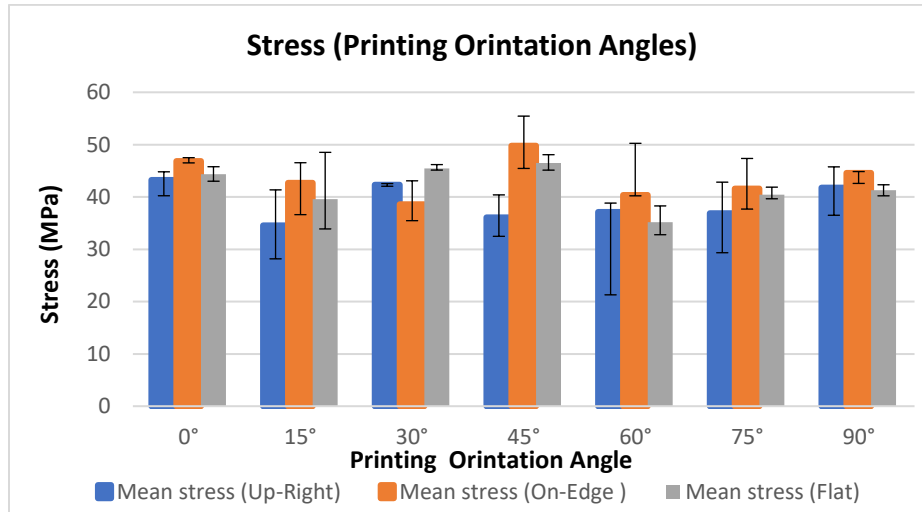


Fig. 17: Comparison of mean tensile strength across different building orientation angles for the three printing directions (Up-Right, On-Edge, Flat).

Strain Comparison (Fig. 18), this plot compares the ductility. The results might be more complex. While Up-Right is expected to have low strain, the comparison between Flat and On-Edge might vary depending on the specific orientation angles being averaged or compared. However, generally, the Flat direction (especially at favorable angles like 0° or 45°) or the On-Edge direction might exhibit higher average strain than the Up-Right direction.

Table 5 Consolidated summary of mean tensile stress and mean strain at failure for ABS samples across all printing directions (Up-Right, On-Edge, Flat) and building orientation angles.

	Mean stress (Up-Right)			Mean Strain (Up-Right)		
Printing orientation angle	Maximum stress (Up-Right)	Mean stress (Up-Right)	Minimum stress (Up-Right)	Maximum strain (Up-Right)	Mean Strain (Up-Right)	Minimum Strain (Up-Right)
0°	44.79986885	43.2527924	40.22252	0.377857	0.337936	0.314059
15°	41.34402855	34.5318655	28.16058	0.54143	0.456722	0.406774
30°	42.55118075	42.328492	42.0403	0.349283	0.330571	0.306435
45°	40.38425909	36.0771387	32.46718	0.407689	0.38559	0.354527
60°	38.83044698	37.1102305	21.28182	0.349778	0.338703	0.333122
75°	42.82393409	36.8999991	29.33452	0.371194	0.352473	0.349778
90°	45.73944789	41.7649974	36.49337	0.376196	0.355275	0.336404
	Mean stress (On-Edge)			Mean Strain (On-Edge)		
Printing Orientation angle	Maximum stress (On-Edge)	Mean stress (On-Edge)	Minimum stress (On-Edge)	Maximum strain (On-Edge)	Mean Strain (On-Edge)	Minimum Strain (On-Edge)
0°	47.50708117	46.852101	46.49843	0.532652	0.499502	0.468227
15°	46.53871768	42.6945235	36.61281	0.622177	0.532237	0.475124
30°	43.07456685	38.6056354	35.45801	0.773567	0.672007	0.617136
45°	55.44939747	49.8183504	45.44803	0.747192	0.67989	0.632397
60°	44.83858554	34.9461952	34.79475	0.601499	0.53568	0.464201
75°	46.18287933	40.3942931	36.51302	0.482175	0.47394	0.458067
90°	45.42021556	45.1400719	43.1492	0.461394	0.42314	0.39276
	Mean stress (Flat)			Mean Strain (Flat)		
Printing Orientation angle	Maximum stress (Flat)	Mean stress (Flat)	Minimum stress (Flat)	Maximum strain (Flat)	Mean Strain (Flat)	Minimum Strain (Flat)
0°	45.77431883	44.3608504	43.00171	0.51209	0.416467	0.366565
15°	48.51707454	39.6009625	33.87641	0.489559	0.460336	0.405909
30°	46.18042364	45.4657614	45.13211	0.443928	0.394409	0.367764
45°	48.06869937	46.5023408	45.1225	0.418196	0.381587	0.33239
60°	38.27249647	35.1805206	32.77211	0.509156	0.460767	0.414906
75°	41.87234016	40.431595	39.64372	0.455675	0.420032	0.394316
90°	42.3230166	41.303953	40.20687	0.438977	0.409334	0.371996

Summary Comparing Orientations at 0°/90° Angle

Table 6 likely provides a focused comparison, extracting the data specifically for the 0° and 90° building orientation angles (or the pairs like 0°/90°, 15°/75° etc. representing parallel/perpendicular extremes) for each of the three printing directions. This allows for a direct comparison of the best-case (load along rasters) and worst-case (load across rasters or layers) scenarios within each build direction, further highlighting the anisotropic behavior.

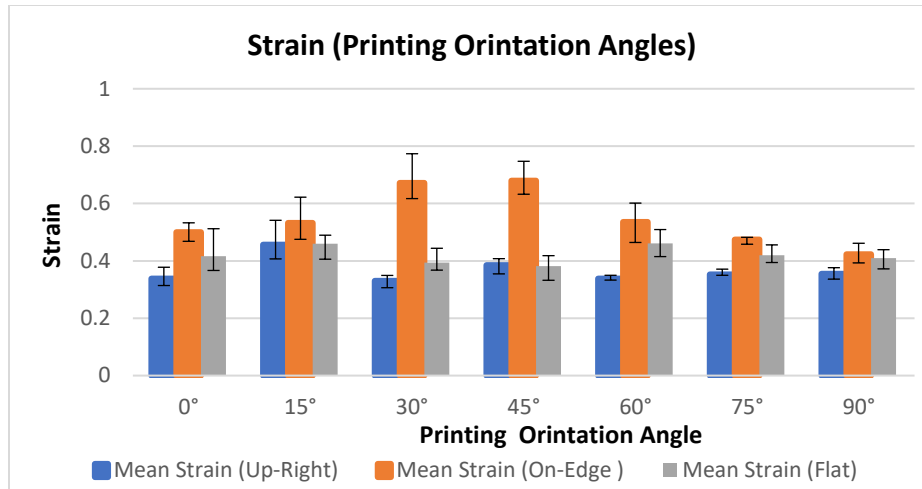


Fig. 18 Comparison of mean strain at failure across different building orientation angles for the three printing directions (Up-Right, On-Edge, Flat).

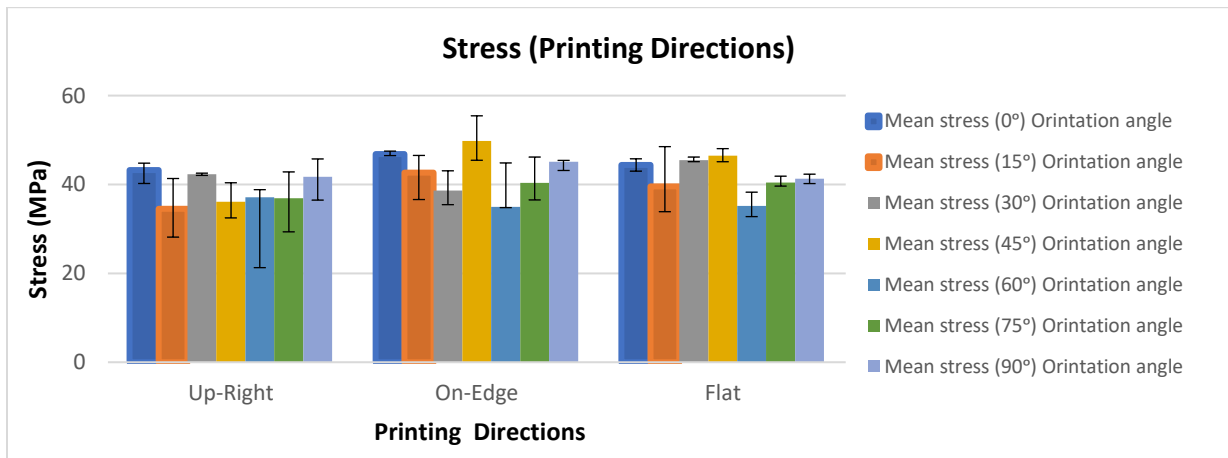


Fig. 19: Bar chart summarizing the effect of printing direction (Up-Right, On-Edge, Flat) on the mean tensile strength of ABS printed samples, averaged across orientation angles.

Figure 19 presents a bar chart comparing the mean tensile strength for each printing direction, potentially averaged across all orientation angles or showing the range. Figure 20 shows a similar bar chart for the mean strain at failure. These figures provide a high-level visual summary of the findings presented in Figs 17 and 18 and Table 5, emphasizing the overall performance differences between the Up-Right, On-Edge, and Flat printing strategies. They clearly depict the superior strength generally achieved in the Flat direction and the significantly lower strength in the Up-Right direction.

Table 6 Comparison of mean tensile properties (stress and strain) for ABS samples printed in different directions at key building orientation angles (e.g., 0° vs 90°).

	Mean stress (0°) Orientation angle			Mean Strain (0°) Orientation angle		
Printing Direction	Maximum stress (0°) Orientation angle	Mean stress (0°) Orientation angle	Minimum stress (0°) Orientation angle	Maximum strain (0°) Orientation angle	Mean Strain (0°) Orientation angle	Minimum Strain (0°) Orientation angle
Up-Right	44.79987	43.25279	40.22252	0.377857	0.337936	0.314059
On-Edge	47.50708	46.8521	46.49843	0.532652	0.499502	0.468227
Flat	45.77432	44.36085	43.00171	0.51209	0.416467	0.366565
	Mean stress (15°) Orientation angle			Mean Strain (15°) Orientation angle		
Printing Direction	Maximum stress (15°) Orientation angle	Mean stress (15°) Orientation angle	Minimum stress (15°) Orientation angle	Maximum strain (15°) Orientation angle	Mean Strain (15°) Orientation angle	Minimum Strain (15°) Orientation angle
Up-Right	41.34403	34.53187	28.16058	0.54143	0.456722	0.406774
On-Edge	46.53872	42.69452	36.61281	0.622177	0.532237	0.475124
Flat	48.51707	39.60096	33.87641	0.489559	0.460336	0.405909
	Mean stress (30°) Orientation angle			Mean Strain (30°) Orientation angle		
Printing Direction	Maximum stress (30°) Orientation angle	Mean stress (30°) Orientation angle	Minimum stress (30°) Orientation angle	Maximum strain (30°) Orientation angle	Mean Strain (30°) Orientation angle	Minimum Strain (30°) Orientation angle
Up-Right	42.55118	42.32849	42.0403	0.349283	0.330571	0.306435
On-Edge	43.07457	38.60564	35.45801	0.773567	0.672007	0.617136
Flat	46.18042	45.46576	45.13211	0.443928	0.394409	0.367764
	Mean stress (45°) Orientation angle			Mean Strain (45°) Orientation angle		
Printing Direction	Maximum stress (45°) Orientation angle	Mean stress (45°) Orientation angle	Minimum stress (45°) Orientation angle	Maximum strain (45°) Orientation angle	Mean Strain (45°) Orientation angle	Minimum Strain (45°) Orientation angle
Up-Right	40.38426	36.07714	32.46718	0.407689	0.38559	0.354527
On-Edge	55.4494	49.81835	45.44803	0.747192	0.67989	0.632397
Flat	48.0687	46.50234	45.1225	0.418196	0.381587	0.33239
	Mean stress (60°) Orientation angle			Mean Strain (60°) Orientation angle		
Printing Direction	Maximum stress (60°) Orientation angle	Mean stress (60°) Orientation angle	Minimum stress (60°) Orientation angle	Maximum strain (60°) Orientation angle	Mean Strain (60°) Orientation angle	Minimum Strain (60°) Orientation angle
Up-Right	38.83045	37.11023	21.28182	0.349778	0.338703	0.333122
On-Edge	44.83859	34.9462	34.79475	0.601499	0.53568	0.464201
Flat	38.2725	35.18052	32.77211	0.509156	0.460767	0.414906
	Mean stress (75°) Orientation angle			Mean Strain (75°) Orientation angle		
Printing Direction	Maximum stress (75°) Orientation angle	Mean stress (75°) Orientation angle	Minimum stress (75°) Orientation angle	Maximum strain (75°) Orientation angle	Mean Strain (75°) Orientation angle	Minimum Strain (75°) Orientation angle
Up-Right	42.82393	36.9	29.33452	0.371194	0.352473	0.349778
On-Edge	46.18288	40.39429	36.51302	0.482175	0.47394	0.458067
Flat	41.87234	40.4316	39.64372	0.455675	0.420032	0.394316
	Mean stress (90°) Orientation angle			Mean Strain (90°) Orientation angle		

Printing Direction	Maximum stress (90°) Orientation angle	Mean stress (90°) Orientation angle	Minimum stress (90°) Orientation angle	Maximum strain (90°) Orientation angle	Mean Strain (90°) Orientation angle	Minimum Strain (90°) Orientation angle
Up-Right	45.73945	41.765	36.49337	0.376196	0.355275	0.336404
On-Edge	45.42022	45.14007	43.1492	0.461394	0.42314	0.39276
Flat	42.32302	41.30395	40.20687	0.438977	0.409334	0.371996

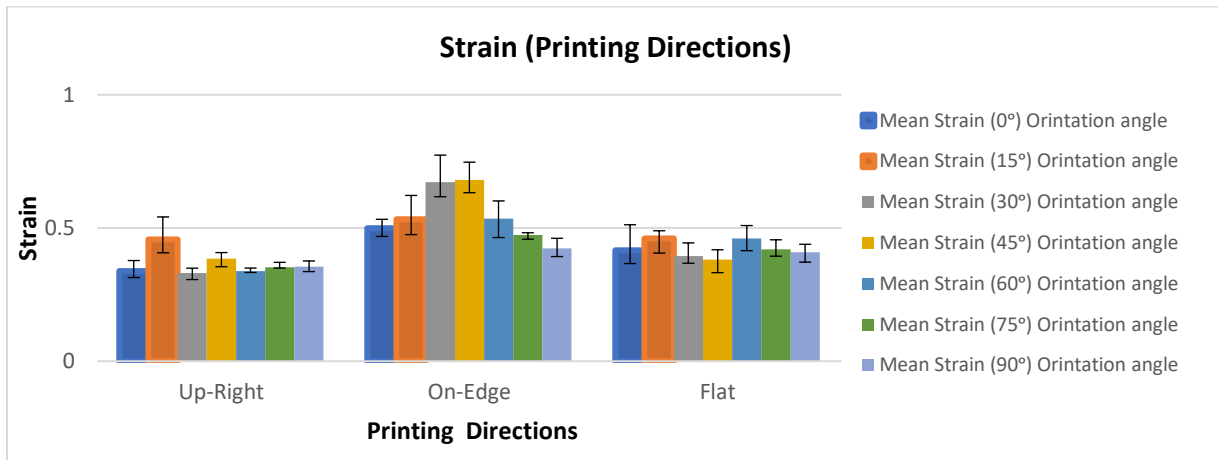


Fig. 20 Bar chart summarizing the effect of printing direction (Up-Right, On-Edge, Flat) on the mean strain at failure of ABS printed samples, averaged across orientation angles.

Fractographic assessment

Scanning Optical Microscopy (SOM) plays a crucial role in the post-failure analysis of Fused Filament Fabrication (FFF) specimens. This technique provides valuable visual information about the fracture surface morphology at magnifications typically sufficient to observe key features inherent to the FFF process. By examining the fracture surface, SOM allows for the identification of characteristics such as the distinct layer lines resulting from the additive manufacturing process, the presence and distribution of voids (both within rasters and between layers), and evidence of filament deformation or pull-out. It helps differentiate between failure modes, such as brittle fracture characterized by relatively smooth surfaces with minimal deformation, and more ductile failure indicated by signs of filament stretching or necking. While SOM offers lower resolution and magnification compared to Scanning Electron Microscopy (SEM), it provides a readily accessible method for initial qualitative assessment, correlating observable microstructural features like layer adhesion quality and void density with the processing parameters (like build orientation and raster angle) and the resulting mechanical performance observed during testing.

Fractographic assessment involves the detailed analysis and interpretation of fracture surfaces to understand the mechanisms of failure in materials. For FFF-printed ABS components, this assessment is critical because the layer-by-layer construction inherently introduces specific microstructural features that dictate failure pathways. Key features examined include delamination, which is the separation between printed

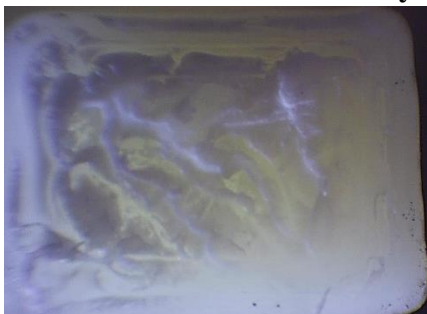
layers and is often the primary failure mode when tensile loads are applied perpendicular to the layers (Z-direction or Up-Right orientation), indicating relatively weak inter-layer bonding. Voids are another critical feature, often observed between adjacent extruded filaments (rasters) within a layer, or at the interface between layers. These voids act as stress concentrators, initiating cracks and reducing the load-bearing cross-sectional area. The appearance of the fractured filaments themselves – whether they show signs of ductile stretching and necking or clean, brittle breaks – provides further information about the failure mode. By correlating these fractographic features (evident in Figs 21-23 of your draft) with printing directions and orientations, we can directly link processing choices to the material's resistance to crack initiation and propagation, explaining the observed anisotropy in mechanical properties like tensile strength and strain at failure. For instance, smoother fracture surfaces with fewer voids generally correspond to better fusion and higher strength (often seen in Flat or On-Edge orientations compared to Up-Right), while rougher surfaces might indicate more energy absorption before failure or significant void presence.

These figures display optical microscopy images of the fracture surfaces for samples printed in the Up-Right (Fig. 21), On-Edge (Fig. 22), and Flat (Fig. 23) directions, likely showing examples from various orientation angles within each.

Figure 21 (Up-Right), images would typically show clear evidence of layer delamination, with relatively flat fracture surfaces running parallel to the build plate. Few signs of significant filament stretching might be visible, indicating brittle inter-layer failure.

Figure 22 (On-Edge), fracture surfaces might appear more complex, potentially showing vertical lines corresponding to the interfaces between adjacent extruded filaments. Depending on the orientation angle, evidence of filament fracture or shearing between filaments might be visible. Voids between rasters could be apparent.

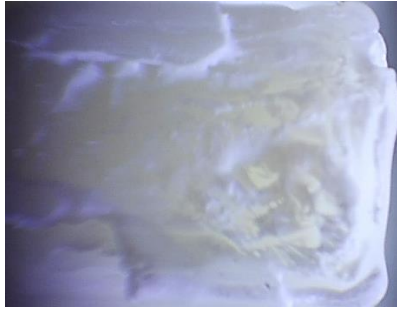
Figure 23 (Flat), these images would vary significantly with orientation angle. For angles near 0° , fractured filament ends with some ductile drawing might be seen. For angles near 90° , the fracture path would likely run between adjacent rasters, showing the semi-circular profiles of the filaments. For 45° , a mix of filament breakage and inter-raster failure might occur. Voids between rasters are often visible. These images support the mechanical test data by visualizing the failure mechanisms.



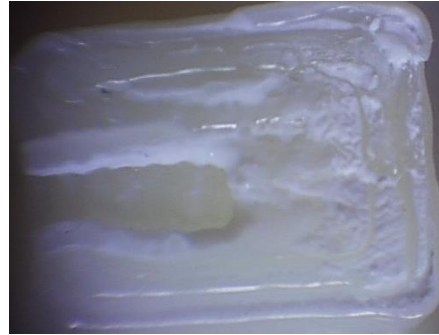
(a) 61_Up-right_Angle_0-90



(b) 64_Up-right_Angle_15-75

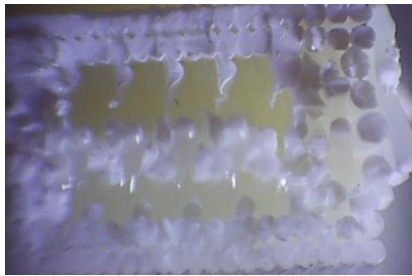


(c) 67_Up-right_Angle_30-60

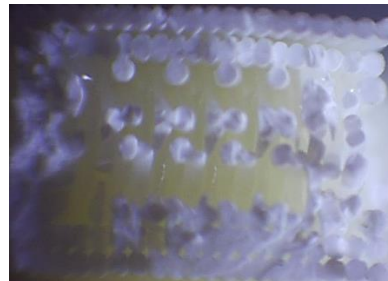


(d) 70_Up-right_Angle_45

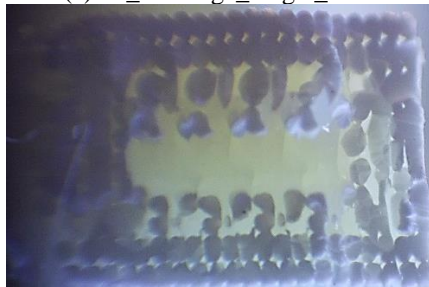
Fig. 21 Optical microscopy images of fracture surfaces for FFF tensile samples printed in the Up-Right direction at various orientation angles (e.g., (a) $[0^\circ, 90^\circ]$, (b) $[15^\circ, 75^\circ]$, (c) $[30^\circ, 60^\circ]$, (d) $[45^\circ/-45^\circ]$).



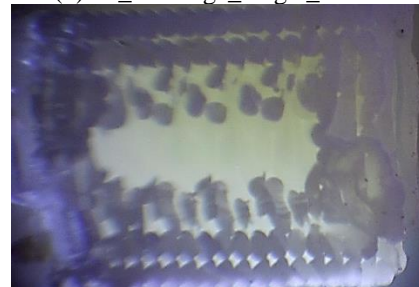
(a) 37_On-Edge_Angle_0-90



(b) 40_On-Edge_Angle_15-75

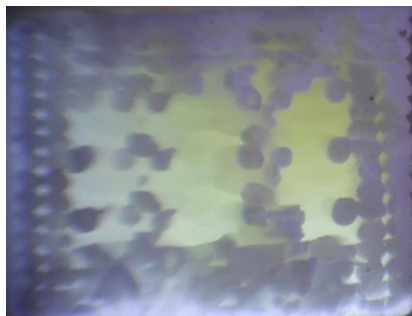


(c) 43_On-Edge_Angle_30-60

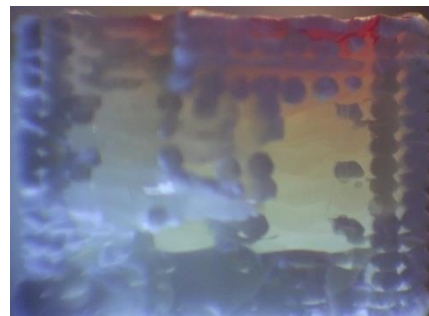


(d) 46_On-Edge_Angle_45

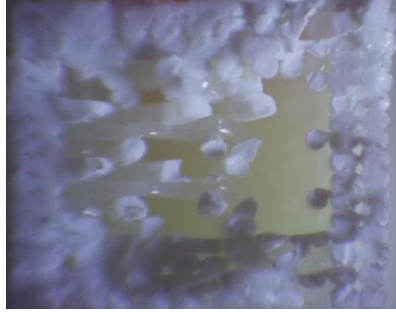
Fig. 22 Optical microscopy images of fracture surfaces for FFF tensile samples printed in the On-Edge direction at various orientation angles (e.g., (a) $[0^\circ, 90^\circ]$, (b) $[15^\circ, 75^\circ]$, (c) $[30^\circ, 60^\circ]$, (d) $[45^\circ/-45^\circ]$).



(a) 13_Flat_Angle_0-90



(b) 16_Flat_Angle_15-75



(c) 19_Flat_Angle_30-60



(d) 22_Flat_Angle_45

Fig. 23 Optical microscopy images of fracture surfaces for FFF tensile samples printed in the Flat direction at various orientation angles (e.g., (a) $[0^\circ, 90^\circ]$, (b) $[15^\circ, 75^\circ]$, (c) $[30^\circ, 60^\circ]$, (d) $[45^\circ/-45^\circ]$).

DISCUSSION

Mechanistic Origins of Anisotropic Strength and Ductility

The systematically observed anisotropy in both the tensile strength and ductility of FFF-processed ABS fundamentally originates from the distinct structural features created at different length scales by the manufacturing process [20, 21 and 38]. The cornerstone of this anisotropy lies in the differential strength of material cohesion: the intrinsic strength along the axis of an extruded filament (intra-raster) versus the adhesion formed at the interfaces between adjacent filaments, either side-by-side within a layer (inter-raster) or stacked in successive layers (inter-layer) [5, 23, 39 and 40]. Inter-layer and inter-raster bonds are formed primarily via thermal fusion during a limited time window, relying on localized polymer reheating and chain interdiffusion, [23, 39 and 40]. This process seldom achieves the bulk cohesive strength of the continuously processed polymer within the filament, [20, 23]. Consequently, when tensile loads directly challenge these interfaces, failure occurs preferentially. This is most dramatically illustrated by the Up-Right printing direction, where loading perpendicular to the layers targets the weakest inter-layer bonds, resulting in low UTS and characteristically brittle failure via delamination, hence minimal ductility (low strain at failure), [23], a finding strongly supported by our results (Figs 7, 8, 21). Similarly, within the Flat printing direction, the significant drop in strength and potentially ductility observed at a 90° raster orientation angle occurs because the load must be transferred across the relatively weak inter-raster bonds, [41]. Conversely, the superior strength at a 0° raster angle arises from loading along the intrinsically stronger continuous filaments [40, 41].

Interdependence of Direction, Raster Angle, Strength, and Ductility

This study clearly demonstrates that printing direction and raster orientation angle are not independent factors but interact to determine the final tensile behavior and ductility. The printing direction sets the overall context and performance ceiling by dictating which type of interface (inter-layer vs. inter-raster) is primarily stressed or bypassed. The Up-Right direction is inherently limited by inter-layer weakness, rendering raster angle effects secondary for both strength and ductility (Figs 7, 8). The On-Edge direction removes the direct inter-layer tensile loading, leading to improved strength, but performance becomes highly sensitive to the raster

orientation angle within the vertical layers, affecting both strength and ductility (Figs 11, 12). The Flat direction offers the highest strength potential by allowing direct loading along filaments (0° angle), but it also exhibits the most pronounced sensitivity to raster orientation angle for both strength and ductility (Figs 15, 16). A key finding is the potential strength-ductility trade-off, particularly evident in the Flat direction: the 0° angle maximizes strength but may not maximize ductility, whereas the $\pm 45^\circ$ angle, while sacrificing some strength, might enhance ductility by promoting energy-absorbing shear deformation mechanisms between rasters, [41]. This interplay necessitates a nuanced approach to orientation selection based on specific application demands.

Ductility and Failure Mechanisms

The strain at failure, representing the material's ductility, also exhibited significant anisotropy, often correlating inversely with strength in brittle failure modes but showing more complex behavior otherwise. The Up-Right direction consistently showed low strain values (Figs 8, 18, and 20; Table 2, 5), consistent with the brittle nature of delamination, [23]. The Flat and On-Edge directions displayed a wider range of ductility dependent on the raster angle (Figs 12, 16, 18, and 20; Tables 3, 4, 5). Notably, intermediate raster angles (e.g., 45° in the Flat direction) sometimes yield higher ductility compared to 0° or 90° , potentially due to the activation of shear yielding mechanisms between rasters, which can absorb more energy before failure, [41]. The fractographic evidence supports this interpretation: smoother surfaces indicative of rapid crack propagation (brittle failure) might correspond to low strain conditions (e.g., Up-Right, 90° Flat), while rougher surfaces with evidence of filament stretching or pull-out suggest more energy absorption and higher ductility (e.g., potentially 0° or 45° Flat) [42]. The presence of voids, visible in fractographs (Figs 22 and 23), inevitably acts as stress concentrators and crack initiation sites, reducing both strength and potentially ductility compared to an ideal, fully dense material, [42, 43].

Role of Microstructure: Voids and Interface Quality

While the geometric arrangement defined by direction and raster angle provides the primary framework for anisotropy, the actual mechanical performance is further modulated by microstructural features inherent to the FFF process, such as voids and variations in interface fusion quality, [42, 43]. Voids are almost unavoidable, arising from the packing geometry of near-cylindrical rasters and potential material shrinkage, [43]. These defects, whether between layers or between rasters, reduce the load-bearing area and act as potent stress concentrators, potentially triggering crack initiation at lower applied stresses and limiting overall strength and ductility, [42, 44]. The quality of fusion at the interfaces is equally critical and depends heavily on the thermal history (temperature, cooling rate) [36, 45 and 46]. Poor fusion results in weak bonds that fail easily, amplifying the negative effects of unfavorable orientations and reducing both strength and deformation capacity. Our fractographic analysis (Figs 21-23) provided visual evidence of these features – the presence of voids, particularly between rasters in Flat/OE samples, and the differing fracture surface morphologies suggesting variations in bond strength (e.g., clean delamination vs.

rougher, more tortuous paths) – which directly correlate with the measured variations in tensile strength and ductility across the different printing configurations.

Contextualizing Strength and Ductility Findings

The observed trends – the clear strength hierarchy by printing direction (Flat > On-Edge > Up-Right), the strong influence of raster angle on in-plane strength and ductility, and the specific weakness and brittleness of the Up-Right orientation – are highly consistent with the broad consensus in the FFF literature for ABS and similar thermoplastics, [9 - 11, 21, 22, 24, 27, 40 and 41]. The specific UTS and strain values obtained (on MPa values and % strain) likely fall within expected bounds for FFF-ABS processed under moderate infill conditions, [34, 46], although direct comparison requires caution due to material and process variations between studies. This research contributes by providing a particularly systematic and comprehensive dataset that maps both strength and ductility across the full matrix of three primary directions and multiple raster angles (0° to 90°), offering a more detailed picture than studies limited to fewer orientations. The explicit coupling of this mechanical data with orientation-specific fractography enhances the mechanistic interpretation of why both strength and ductility vary so significantly. This detailed understanding of static tensile behavior and deformation limits is also crucial foundational knowledge for predicting performance under more complex scenarios like fatigue loading, where crack initiation and propagation are heavily influenced by these same anisotropic features and interface weaknesses, [3, 45, 47 and 48].

Design Implications: Optimizing Strength versus Ductility

The results carry significant practical implications for the design and manufacturing workflow of FFF-ABS parts intended for functional use. It is evident that part orientation is a critical design variable that must be consciously chosen to meet performance requirements, considering both strength and ductility.

Prioritizing Strength, if maximum load-bearing capacity in tension is the primary goal, the part should be oriented in the Flat direction with the raster angle aligned as closely as possible to 0° relative to the major tensile stress axis.

Prioritizing Ductility/Toughness, if resistance to fracture under deformation, energy absorption, or tolerance to stress concentrations is more critical than absolute strength, orienting the part in the Flat direction with a ±45° raster angle may be advantageous, potentially offering higher strain at failure, although likely at the cost of reduced UTS compared to the 0° orientation.

Intermediate Performance, the On-Edge direction can provide a viable alternative when Flat orientation is not feasible due to geometry or support structure considerations, but careful selection of the raster angle is needed to optimize its intermediate strength and ductility.

Avoiding Critical Weakness, the Up-Right direction should be actively avoided for

components where either significant tensile strength *or* appreciable ductility is required, as this orientation inherently combines the lowest strength with the most brittle failure mode (delamination).

This study provides the empirical basis for engineers to make these informed orientation choices, moving beyond simple strength maximization to consider the crucial aspect of ductility and failure behavior.

CONCLUSIONS

This study provided a comprehensive experimental characterization of the anisotropic uniaxial tensile behavior and ductility of Acrylonitrile Butadiene Styrene (ABS) parts fabricated via Fused Filament Fabrication (FFF), focusing on the distinct roles of printing direction (Up-Right, On-Edge, Flat) and building orientation angle (raster angle, 0° to 90°). The investigation confirms that FFF-ABS exhibits profound mechanical anisotropy, impacting both its load-carrying capacity and its ability to deform before fracture. The principal conclusions are:

- 1. Pronounced Anisotropy Confirmed:** The mechanical properties, particularly Ultimate Tensile Strength (UTS) and Strain at Failure, exhibited strong dependence on both the primary build direction and the in-plane raster angle, confirming the significant anisotropy inherent to the FFF process for ABS. This necessitates careful consideration of orientation during design for load-bearing applications.
- 2. Hierarchy of Strength by Build Direction:** A clear hierarchy in tensile strength based on build direction was established: specimens printed in the Flat orientation demonstrated the highest potential strength, followed by the On-Edge orientation, with the Up-Right orientation being markedly the weakest. This highlights the critical limitation imposed by inter-layer bond strength when tensile loads are applied perpendicular to the build layers.
- 3. Significant Impact of Raster Angle:** Within the stronger Flat and On-Edge printing directions, the building orientation angle (raster angle relative to the load axis) played a crucial role. For Flat specimens, aligning rasters nearly parallel to the tensile load (0° angle) resulted in the maximum UTS, while perpendicular alignment (90° angle) yielded the lowest strength within that plane. This underscores the ability to tailor in-plane properties through deliberate raster strategy selection.
- 4. Correlation with Failure Mechanisms:** Fractographic analysis using optical microscopy supported the mechanical findings by revealing distinct failure modes for different orientations. Delamination was characteristic of the weak Up-Right direction, while varying degrees of inter-raster separation and intra-raster (filament) fracture were observed in On-Edge and Flat specimens, correlating well with the measured strength and ductility variations.
- 5. Practical Design Implications:** The quantitative data and qualitative observations strongly emphasize that part orientation is a critical design parameter for FFF-ABS. To maximize tensile performance and reliability, designers should prioritize orienting parts such that critical loads align with the strongest configuration (typically Flat, with rasters parallel to the load). Loading perpendicular to the layers (Up-Right) should be avoided in structural applications whenever feasible.

By systematically mapping both tensile strength and ductility across a wide range of orientations and correlating these with failure modes, this research provides crucial empirical data and reinforces the understanding needed for optimizing the design and fabrication of reliable FFF-printed ABS components.

In essence, this research provides detailed empirical evidence reinforcing the anisotropic nature of FFF-printed ABS and quantifies the specific effects of build direction and raster angle on tensile performance. These findings offer valuable guidance for engineers and designers, enabling more informed decisions regarding part orientation to better exploit the capabilities of FFF technology while mitigating the risks associated with its inherent directional weaknesses, ultimately leading to more robust and reliable 3D-printed ABS components. Future work focusing on interactions with other process parameters, different loading modes, and advanced material modeling will further enhance the predictive design capabilities for this widely used manufacturing process.

REFERENCES

1. Khorasani M., Ghasemi A., B. Rolfe B., and Gibson I., “Additive manufacturing a powerful tool for the aerospace industry,” *Rapid Prototyp. J.*, Vol. 28, No. 1, pp. 87–100, Jan. (2022), doi: 10.1108/RPJ-01-2021-0009.
2. Ali M. H., Issayev G., Shehab E., and Sarfraz S., “A critical review of 3D printing and digital manufacturing in construction engineering,” *Rapid Prototyp. J.*, Vol. 28, no. 7, pp. 1312–1324, Jun. 2022, doi: 10.1108/RPJ-07-2021-0160.
3. Rajaguru K., Karthikeyan T., and Vijayan V., “Additive manufacturing – State of art,” *Mater. Today Proc.*, Vol. 21, pp. 628–633, (2020), doi: 10.1016/j.matpr.2019.06.728.
4. Rouf S., Malik A., Singh N., Raina A., Naveed N., Siddiqui M. I., and Haq M. I., “Additive manufacturing technologies: Industrial and medical applications,” *Sustain. Oper. Comput.*, Vol. 3, pp. 258–274, (2022), doi: 10.1016/j.susoc.2022.05.001.
5. Vanaei S., Parizi M. S., Vanaei S., Saleemizadehparizi F., and Vanaei H. R., “An Overview on Materials and Techniques in 3D Bioprinting Toward Biomedical Application,” *Eng. Regen.*, Vol. 2, pp. 1–18, (2021), doi: 10.1016/j.engreg.2020.12.001.
6. Lindemann C., Reiher T., Jahnke U., and Koch R., “Towards a sustainable and economic selection of part candidates for additive manufacturing,” *Rapid Prototyp. J.*, Vol. 21, No. 2, pp. 216–227, Mar. (2015), doi: 10.1108/RPJ-12-2014-0179.
7. Vyavahare S., Teraiya S., Panghal D., and Kumar S., “Fused deposition modelling: a review,” *Rapid Prototyp. J.*, Vol. 26, No. 1, pp. 176–201, Jan. (2020), doi: 10.1108/RPJ-04-2019-0106.
8. Gibson I., Rosen D. W., and Stucker B., *Additive Manufacturing Technologies*. Boston, MA: Springer US, (2010). doi: 10.1007/978-1-4419-1120-9.
9. Petrov M. A. and El-Deeb I. S. A., “Experimental and numerical investigations of mechanical properties of 3D-printed polymeric samples with ideal and roughed surfaces,” *AIP Conf. Proc.* 2113, 150021, p. 150021, (2019), doi: 10.1063/1.5112697.
10. Dawoud M., Taha I., and Ebeid S. J., “Mechanical behaviour of ABS: An experimental study using FDM and injection moulding techniques,” *J. Manuf. Process.*, Vol. 21, pp. 39–45, Jan. (2016), doi: 10.1016/j.jmapro.2015.11.002.

11. Ahn S., Montero M., Odell D., Roundy S., and Wright P. K., "Anisotropic material properties of fused deposition modeling ABS," *Rapid Prototyp. J.*, Vol. 8, No. 4, pp. 248–257, Oct. (2002), doi: 10.1108/13552540210441166.
12. Es-Said O. S., Foyos J., Noorani R., Mendelson M., Marloth R., and Pregger B. A., "Effect of Layer Orientation on Mechanical Properties of Rapid Prototyped Samples," *Mater. Manuf. Process.*, Vol. 15, No. 1, pp. 107–122, Jan. (2000), doi: 10.1080/10426910008912976.
13. Yang C., Tian X., Li D., Cao Y., Zhao F., and Shi C., "Influence of thermal processing conditions in 3D printing on the crystallinity and mechanical properties of PEEK material," *J. Mater. Process. Technol.*, Vol. 248, pp. 1–7, Oct. (2017), doi: 10.1016/j.jmatprotec.2017.04.027.
14. Lee B. H., Abdullah J., and Khan Z. A., "Optimization of rapid prototyping parameters for production of flexible ABS object," *J. Mater. Process. Technol.*, Vol. 169, No. 1, pp. 54–61, Oct. (2005), doi: 10.1016/j.jmatprotec.2005.02.259.
15. Croccolo D., De Agostinis M., and Olmi G., "Experimental characterization and analytical modelling of the mechanical behaviour of fused deposition processed parts made of ABS-M30," *Comput. Mater. Sci.*, Vol. 79, pp. 506–518, Nov. (2013), doi: 10.1016/j.commatsci.2013.06.041.
16. Lee C. S., Kim S. G., Kim H. J., and Ahn S. H., "Measurement of anisotropic compressive strength of rapid prototyping parts," *J. Mater. Process. Technol.*, Vol. 187–188, pp. 627–630, Jun. (2007), doi: 10.1016/j.jmatprotec.2006.11.095.
17. Rezaeian P., Ayatollahi M. R., Nabavi-Kivi A., and Razavi N., "Effect of printing speed on tensile and fracture behavior of ABS specimens produced by fused deposition modeling," *Eng. Fract. Mech.*, Vol. 266, p. 108393, May (2022), doi: 10.1016/j.engfracmech.2022.108393.
18. Sood A. K., Ohdar R. K., and Mahapatra S. S., "Parametric appraisal of mechanical property of fused deposition modelling processed parts," *Mater. Des.*, Vol. 31, No. 1, pp. 287–295, Jan. (2010), doi: 10.1016/j.matdes.2009.06.016.
19. Dhinesh S. K., Arun P. S., Senthil K. K. L., and Megalingam A., "Study on flexural and tensile behavior of PLA, ABS and PLA-ABS materials," *Mater. Today Proc.*, Vol. 45, pp. 1175–1180, (2021), doi: 10.1016/j.matpr.2020.03.546.
20. Ahn S. H., Baek C., Lee S., and Ahn I. S., "Anisotropic Tensile Failure Model of Rapid Prototyping Parts - Fused Deposition Modeling (FDM)," *Int. J. Mod. Phys. B*, Vol. 17, No. 08n09, pp. 1510–1516, Apr. (2003), doi: 10.1142/S0217979203019241.
21. Wu W., Geng P., Li G., Zhao D., Zhang H., and Zhao J., "Influence of Layer Thickness and Raster Angle on the Mechanical Properties of 3D-Printed PEEK and a Comparative Mechanical Study between PEEK and ABS," *Materials (Basel)*, Vol. 8, No. 9, pp. 5834–5846, Sep. (2015), doi: 10.3390/ma8095271.
22. Tymrak B. M., Kreiger M., and Pearce J. M., "Mechanical properties of components fabricated with open-source 3-D printers under realistic environmental conditions," *Mater. Des.*, Vol. 58, pp. 242–246, Jun. (2014), doi: 10.1016/j.matdes.2014.02.038.
23. Bellini A. and Güçeri S., "Mechanical characterization of parts fabricated using fused deposition modeling," *Rapid Prototyp. J.*, Vol. 9, No. 4, pp. 252–264, Oct. (2003), doi: 10.1108/13552540310489631.
24. Rajpurohit S. R. and Dave H. K., "Analysis of tensile strength of a fused

filament fabricated PLA part using an open-source 3D printer,” *Int. J. Adv. Manuf. Technol.*, Vol. 101, No. 5–8, pp. 1525–1536, Apr. (2019), doi: 10.1007/s00170-018-3047-x.

25. Esmael E. G., Showaib E. A., and ELDeeb I. S., “Investigating Different Personalized 3D Printable Cast Models for Arm Fractures: Part 1-Finite Element Analysis,” *J. Eng. Research.*, Vol. 8, No. 3, pp. 1–9, (2024).

26. El-Deeb I. S., Grabowik C., Esmael E., Nabhan A., Rashad M., and Ebied S., “Investigation of Effect of Part-Build Directions and Build Orientations on Tension–Tension Mode Fatigue Behavior of Acrylonitrile Butadiene Styrene Material Printed Using Fused Filament Fabrication Technology,” *Materials*, Vol. 17, No. 20. (2024). doi: 10.3390/ma17205133.

27. Petrov M. A. and El-Deeb I. S. A., “Applying 3D-Scan Systems RangeVision for Precision Preparing of Polygonal 3D-Models,” in *2020 International Conference on Industrial Engineering, Applications and Manufacturing (ICIEAM)*, IEEE, pp. 1–6, May (2020), doi: 10.1109/ICIEAM48468.2020.9112038.

28. El-Deeb I. S., Petrov M. A., Grabowik C., Esmael E. G., Rashad M., and Ebied S., “Mechanical Properties of PLA Printed Samples in Different Printing Directions and Orientations Using Fused Filament Fabrication, Part 1: Methodology BT - Intelligent Systems in Production Engineering and Maintenance III,” *Springer Nature Switzerland*, pp. 643–657, (2024). doi: https://doi.org/10.1007/978-3-031-44282-7_49.

29. El-Deeb I. S., Petrov M. A., Grabowik C., Esmael E. G., Rashad M., and Ebied S., “Mechanical Properties of PLA Printed Samples in Different Printing Directions and Orientations Using Fused Filament Fabrication, Part 2: Experimental Research BT - Intelligent Systems in Production Engineering and Maintenance III,” *Springer Nature Switzerland*, pp. 627–642, (2024). doi: https://doi.org/10.1007/978-3-031-44282-7_48.

30. Showaib E. A. and El-deeb I. S., “Representing Surfaces in Reverse Engineering Using Analogue Signals,” *J. Adv. Sci. Eng. Res.*, Vol. 2, No. 4, pp. 280–290, (2012).

31. Afrose M. F., Masood S. H., Iovenitti P., Nikzad M., and Sbarski I., “Effects of part build orientations on fatigue behaviour of FDM-processed PLA material,” *Prog. Addit. Manuf.*, Vol. 1, No. 1–2, pp. 21–28, Jun. (2016), doi: 10.1007/s40964-015-0002-3.

32. A. Standard, “D638, Standard Test Method for Tensile Properties of Plastics, ASTM International, West Coshoshocken, PA,” (2003).

33. Anand Kumar S. N. Y., “Tensile testing and evaluation of 3D-printed PLA specimens as per ASTM D638 Type IV standard.,” *Innov. Des. Anal. Dev. Pract. Aerosp. Automot. Eng. (I-DAD 2018)*, Vol. 2., No. Springer, Singapore, p. pp: 79-95., (2019).

34. Kostakis V., Niaros V., and Giotitsas C., “Open source 3D printing as a means of learning: An educational experiment in two high schools in Greece,” *Telemat. Informatics*, Vol. 32, No. 1, pp. 118–128, Feb. (2015), doi: 10.1016/j.tele.2014.05.001.

35. Zein I., Hutmacher D. W., Tan K. C., and Teoh S. H., “Fused deposition modeling of novel scaffold architectures for tissue engineering applications,” *Biomaterials*, Vol. 23, No. 4, pp. 1169–1185, Feb. (2002), doi: 10.1016/S0142-

9612(01)00232-0.

36. Agarwal K. M., Shubham P., Bhatia D., Sharma P., Vaid H., and Vajpeyi R., "Analyzing the Impact of Print Parameters on Dimensional Variation of ABS specimens printed using Fused Deposition Modelling (FDM)," *Sensors Int.*, Vol. 3, p. 100149, (2022), doi: 10.1016/j.sintl.2021.100149.
37. Dong Y., Ghataura A., Takagi H., Haroosh H. J., Nakagaito A. N., and Lau K.-T., "Polylactic acid (PLA) biocomposites reinforced with coir fibres: Evaluation of mechanical performance and multifunctional properties," *Compos. Part A Appl. Sci. Manuf.*, Vol. 63, pp. 76–84, Aug. (2014), doi: 10.1016/j.compositesa.2014.04.003.
38. Popescu D., Zapciu A., Amza C., Baciu F., and Marinescu R., "FDM process parameters influence over the mechanical properties of polymer specimens: A review," *Polym. Test.*, Vol. 69, pp. 157–166, Aug. (2018), doi: 10.1016/j.polymertesting.2018.05.020.
39. Masood S. H., Mau K., and Song W. Q., "Tensile Properties of Processed FDM Polycarbonate Material," *Mater. Sci. Forum*, Vol. 654–656, pp. 2556–2559, Jun. (2010), doi: 10.4028/www.scientific.net/MSF.654-656.2556.
40. Mohamed O. A., Masood S. H., and Bhowmik J. L., "Optimization of fused deposition modeling process parameters: a review of current research and future prospects," *Adv. Manuf.*, Vol. 3, No. 1, pp. 42–53, Mar. (2015), doi: 10.1007/s40436-014-0097-7.
41. Rankouhi B., Javadpour S., Delfanian F., and Letcher T., "Failure Analysis and Mechanical Characterization of 3D Printed ABS With Respect to Layer Thickness and Orientation," *J. Fail. Anal. Prev.*, Vol. 16, No. 3, pp. 467–481, Jun. (2016), doi: 10.1007/s11668-016-0113-2.
42. Naveed N., "Investigate the effects of process parameters on material properties and microstructural changes of 3D-printed specimens using fused deposition modelling (FDM)," *Mater. Technol.*, Vol. 36, No. 5, pp. 317–330, Apr. (2021), doi: 10.1080/10667857.2020.1758475.
43. Vanaei H. R., Shirinbayan M., Costa, S. F., Duarte F., Covas J. A., Deligant M., Kelladi S., and Tcharkhtchi A., "Experimental study of <scp>PLA</scp> thermal behavior during fused filament fabrication," *J. Appl. Polym. Sci.*, Vol. 138, No. 4, Jan. 2021, doi: 10.1002/app.49747.
44. Yadav D. K., Srivastava R., and Dev S., "Design & fabrication of ABS part by FDM for automobile application," *Mater. Today Proc.*, Vol. 26, pp. 2089–2093, (2020), doi: 10.1016/j.matpr.2020.02.451.
45. Ansari A. A. and Kamil M., "Effect of print speed and extrusion temperature on properties of 3D printed PLA using fused deposition modeling process," *Mater. Today Proc.*, Vol. 45, pp. 5462–5468, (2021), doi: 10.1016/j.matpr.2021.02.137.
46. Rajan K., Samykano M., Kadirgama K., Harun W. S. W., and Rahman M. M., "Fused deposition modeling: process, materials, parameters, properties, and applications," *Int. J. Adv. Manuf. Technol.*, Vol. 120, No. 3–4, pp. 1531–1570, May (2022), doi: 10.1007/s00170-022-08860-7.
47. Jap N. S. F., Pearce G. M., Hellier A. K., Russell N., Parr W. C., and Walsh W. R., "The effect of raster orientation on the static and fatigue properties of filament deposited ABS polymer," *Int. J. Fatigue*, Vol. 124, pp. 328–337, Jul. (2019), doi: 10.1016/j.ijfatigue.2019.02.042.

48. Shanmugam, V., Das, O., Babu, K., Marimuthu, U., Veerasimman, A., Johnson, D. J., Neisiany, R. E., Hedenqvist, M. S., Ramakrishna, S., and Berto, F., “Fatigue behaviour of FDM-3D printed polymers, polymeric composites and architected cellular materials,” Int. J. Fatigue, Vol. 143, p. 106007, Feb. (2021), doi: 10.1016/j.ijfatigue.2020.106007.